Elastic-Plastic Nonlinear Response of a Space Shuttle External Tank Stringer: Part 2 – Thermal and Mechanical Loadings

Norman F. Knight, Jr.[1]
General Dynamics Information Technology, Herndon, Virginia

Jerry E. Warren[2], and Kenny B. Elliott[3]
NASA Langley Research Center, Hampton, Virginia

Kyongchan Song[4]
ATK Space Division, Langley Research Center, Hampton, Virginia

and

Ivatury S. Raju[5]
NASA Langley Research Center, Hampton, Virginia

Elastic-plastic, large-deflection nonlinear thermo-mechanical stress analyses are performed for the Space Shuttle external tank's intertank stringers. Detailed three-dimensional finite element models are developed and used to investigate the stringer's elastic-plastic response for different thermal and mechanical loading events from assembly through flight. Assembly strains caused by initial installation on an intertank panel are accounted for in the analyses. Thermal loading due to tanking was determined to be the bounding loading event. The cryogenic shrinkage caused by tanking resulted in a rotation of the intertank chord flange towards the center of the intertank, which in turn loaded the intertank stringer feet. The analyses suggest that the strain levels near the first three fasteners remain sufficiently high that a failure may occur. The analyses also confirmed that the installation of radius blocks on the stringer feet ends results in an increase in the stringer capability.

I. Introduction

DURING the filling of the external tank (ET) with cryogenic liquid fuels for the last mission of the Space Shuttle *Discovery*, cracking in the foam on an intertank (IT) panel near the liquid-oxygen (LOX) tank interface was observed.[1] Upon further inspection, it was discovered that not only was the foam cracked, but also two external hat-shaped stringers under that foam on the IT had long cracks along the stringer feet between the fasteners and the stringer sidewall. Detailed three-dimensional (3D) finite element (FE) models are developed and analyzed to investigate the stringer elastic-plastic response and to assess the potential for local failure to develop in the stringer feet.[2] The stringers are subject to assembly strains caused by initial installation on an IT panel. In addition, transient thermal loading occurs in these stringers as the LOX tank fills prior to launch, and other mechanical loading events are present for pre-tanking, pre-launch, and flight loading.

[1] Principal Subject Matter Expert, Structural Mechanics. Fellow AIAA, Fellow ASME.
[2] Aerospace Engineer, Structural Dynamics Branch, Member ASME.
[3] Aerospace Engineer, Systems Integration & Test Branch. Member AIAA.
[4] Structural Analyst, Member AIAA.
[5] NASA Technical Fellow for Structures, NASA Engineering and Safety Center. Fellow AIAA, Member ASME. Member ASCE.

The basic coordinate system for the vehicle is indicated in Fig. 1 with the X-axis running along the vehicle axis. The symbol XT is used to define the longitudinal or axial location along the ET (i.e., T refers to tank). Note that a positive Z value is towards the Orbiter. The ET has three main components as indicated in Fig. 2: the liquid oxygen (LOX or LO_2) tank, the IT, and the liquid hydrogen (LH_2) tank.

The IT shown in Fig. 3 is a stiffened right circular cylindrical shell structure that connects the LH_2 and LOX tanks, and contains the attachment points for the solid rocket boosters (SRBs). The IT is approximately 22.5 feet long and has a diameter of approximately 27.5 feet.[3] The IT shell structure is formed by connecting eight 45° curved panels, where two of these panels are referred to as thrust panels and house the SRB attachment points. The other six panels have external hat-shaped stringers that are fastened to the panel skin, doublers, and chord. These eight panels are assembled together with mechanical fasteners to form the IT structure. The axial position along the ET is given by the coordinate XT in terms of inches. For example, the IT forward chord flange is located at XT = 852.8 inches – this XT location defines the LOX-tank/IT interface.

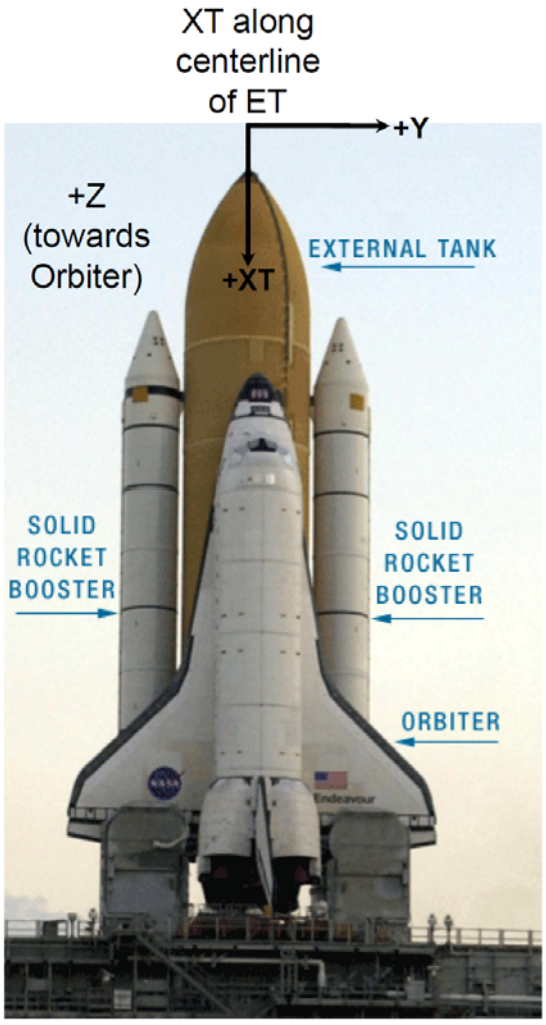

Figure 1. Space Transportation System (STS).

The LOX tank is a thin-walled semi-monocoque shell with four primary sections: a forward ogive, an aft ogive, a cylindrical barrel, and an aft elliptical dome section*, that is closed out with an aft spherical dome cap.[3,4] A portion of the LOX tank was also modeled and incorporated with the IT single-stringer model for the operational thermal and mechanical loading simulations. The present FE 'global' model shown in Fig. 4 includes the LOX tank cylindrical barrel up to but not including the forward T-ring (up to XT = 747.35), the aft elliptical dome including the aft Y-joint and weld lands, and the aft spherical dome cap, thereby enabling the thermo-mechanical structural response simulation of LOX tanking, pre-launch, and flight loading events. The LOX-tank FE model provides stiffness and load introduction to the IT stringer FE for the thermal and mechanical operational loads and was not intended to be a stress analysis model for the LOX tank segments.

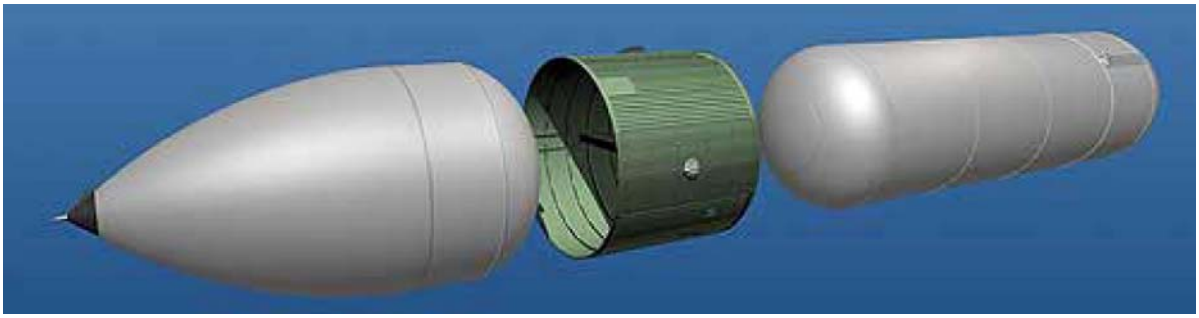

Figure 2. ET basic structural elements (left to right: LOX tank; IT; and LH_2 tank).

* The aft dome is a rib (ring) stiffened shell with increasing stiffener spacing moving from the barrel to the aft dome cap. While not very tall, the eight ribs do exist.

Elastic-plastic, large-deflection nonlinear thermo-mechanical stress analyses are performed for the external hat-shaped stringers (or stiffeners) on the IT portion of the Space Shuttle's ET. These stringers are subject to assembly strains when the stringers are initially installed on an IT panel. Transient thermal loading occurs as the LOX tank fills prior to launch. Other mechanical loading events are also present for pre-tanking, pre-launch, and flight loading events. Detailed 3D FE models are developed and used to investigate the elastic-plastic response of the stringers to operational thermal and mechanical loadings.

The paper summarizes the NASA Engineering and Safety Center (NESC) structural analyses[2] to assess the IT stringer structural response for assembly and thermo-mechanical loading. First, the structural analysis approach is described followed by a discussion of the modeling and analysis process. Then numerical results are presented and discussed. The paper ends with concluding remarks.

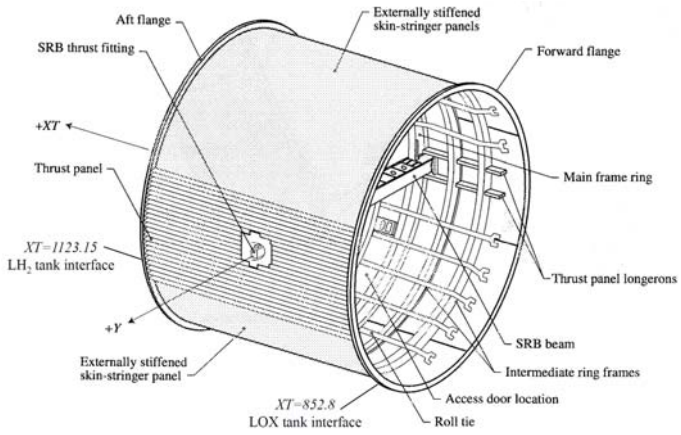

Figure 3. Overview of IT structure (based on Figure 3 in Ref. 2).

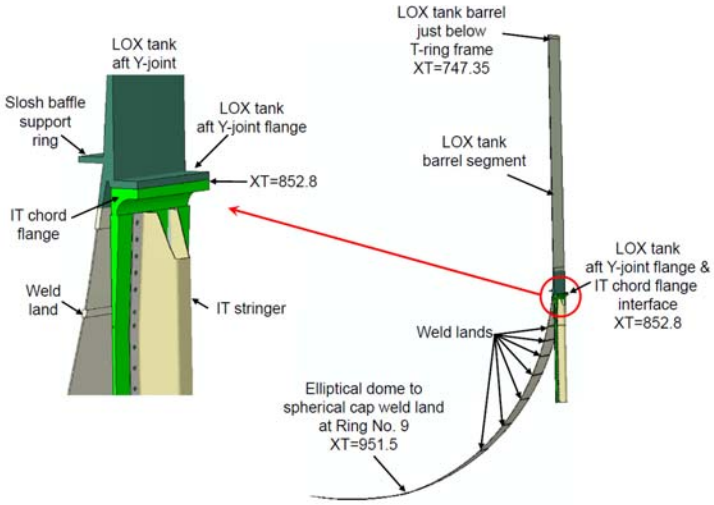

Figure 4. Global model of a 2.5° slice of IT single-stringer and partial LOX tank – aft elliptical dome includes weld lands as indicated.

II. Structural Analysis Approach

The structural analysis approach followed in the IT stringer failure assessment is the building-block approach illustrated in Fig. 5. This building-block approach is used for developing and anchoring detailed FE analyses. All structural analyses are performed using ABAQUS™/Standard*.[5] Analyses of the 3-point bend tests (upper left of Fig. 5) performed at the Langley Research Center (LaRC) served as the anchoring point for several modeling and analysis details. Analyses of the clip tests (upper right of Fig. 5) performed by Lockheed Martin (LM) at the Michoud Assembly Facility (MAF) provided additional correlation data for peak loads and contributed to the formulation of a strain-based failure criterion. Single-stringer models (lower right of Fig. 5) were used to assess various assembly issues including fastener installation sequence, fastener preload, and stringer-feet imperfections. The single-stringer bend test performed at the Marshall Space Flight Center (MSFC) provided test data for model correlation of an assembled stringer and anchored the single-stringer models described in this paper. These single-stringer models were then combined with a partial model of the LOX tank (lower left of Fig. 5), and operational loading cases were evaluated including pre-tanking loading, tanking thermal transient loading, pre-launch loading, and ascent flight loading. Each step in the building-block approach for this application is further described in Ref. 2.

* ABAQUS™/Standard is a registered trademark of Dassault Systèmes Simulia Corp.

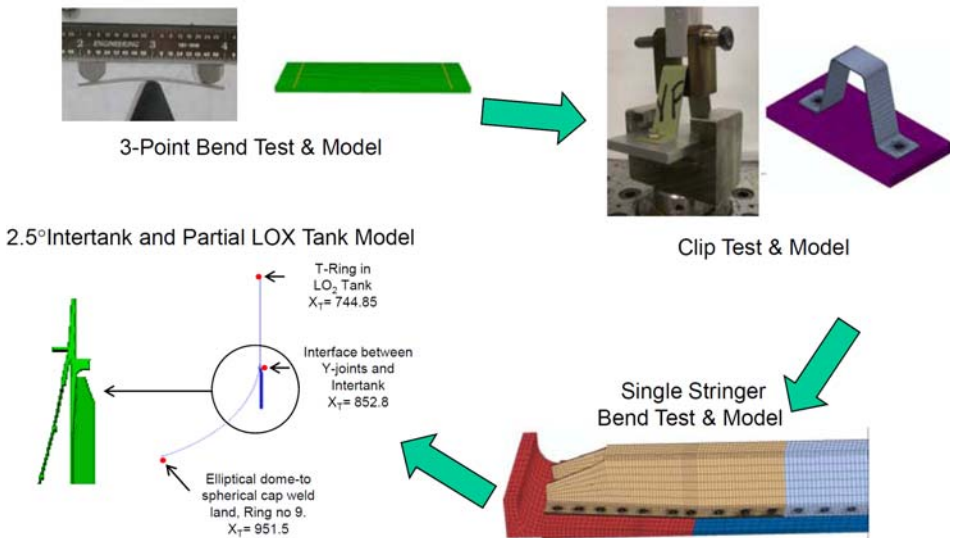

Figure 5. Basic building-block modeling and analysis steps for this assessment.

III. Modeling and Analysis

A. Single-Stringer Modeling

The single-stringer model represents a complete stringer centered within a 2.5° slice of an IT segment at the forward (or LOX tank) end as shown in Fig. 6. The single-stringer model, which has 73,514 C3D8I solid elements and 107,908 nodes, is defined as two independent components: a single hat-shaped stringer and a 2.5° slice of the IT LOX tank end (i.e., IT chord flange, IT skin, and external doublers). In Fig. 6, the tan region represents a typical hat-shaped stringer, and the line within this region on the stringer separates the first ten fasteners nearest the LOX tank end from the aft portion of the stringer model. The forward portion of the stringer model is more refined having four solid elements through the stringer thickness. The green region represents a portion of the IT, which includes the forward chord, panel skin, and doubler components. These model components are assembled using contact and 36 pairs of fasteners. Specific IT skin thickness values and doubler configuration details (i.e., no doublers, a single doubler, or double doublers) depend on the circumferential location of the 2.5° segment around the IT. The two component models are assembled using mostly rivets away from the stringer ends. Near the stringer ends, a combination of GP®* lock bolts and Hi-lok®† fasteners are installed. A cylindrical coordinate system is created and used to assign boundary conditions. Symmetry boundary conditions are imposed on the circumferential faces of the IT model and along the axial end away from the IT chord flange. The IT chord flange surface that mates with the LOX tank flange surface is unconstrained or free.

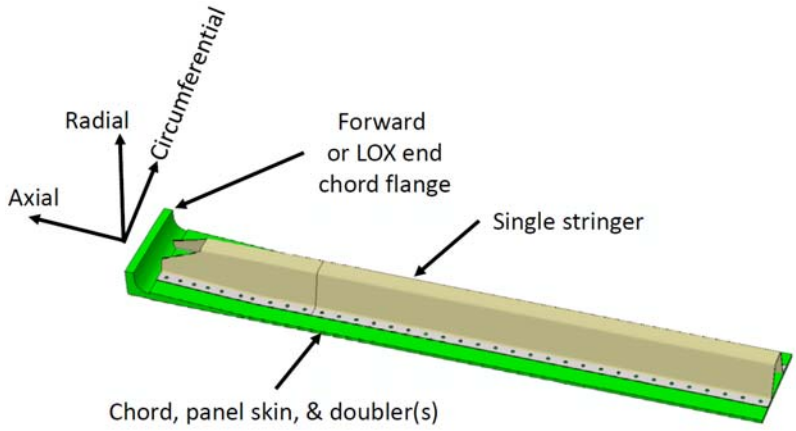

Figure 6. Representative 3D model of a single-stringer configuration: single stringer with portion of the IT (2.5° slice).

The FE mesh for the IT region up to the first ten fasteners has several 8-node C3D8I solid elements through the thickness, and then as the chord runs out, there are only two elements through the thickness of the skin/doubler

* GP® is a registered trademark of Huck International, Inc., Tucson, AZ.
† Hi-lok® is a registered trademark of Hi-Shear Corporation, Torrance, CA.

combination. This transition occurs beyond the region of interest, and results consistent with uniform refinement were confirmed. The hat-shaped IT stringer, denoted by the tan region in Fig. 6, is also independently modeled as a separate structural component. The entire stringer length was initially modeled with four 8-node C3D8I solid elements through the stringer thickness. However, to reduce the computational size of the problem, only a single element through the stringer thickness was used beyond the tenth fastener based on results from mesh convergence studies. The dissimilar FE meshes through the thickness were combined using tied kinematic constraints within ABAQUS™/Standard.[5] These independent FE models are assembled, and surface-to-surface 'hard' contact is assumed between the skin/doubler outer surface and the bottom surface of the stringer feet. Small sliding is permitted, and an aluminum-to-aluminum dry static coefficient of friction is used. The current single-stringer FE model has roughly 1.3 million degrees of freedom (DOF).

The baseline stringer configuration is assumed to be a stringer with flat feet. In this configuration, the stringer feet would sit perfectly on a flat surface; however, because the stringers are installed on the curved IT surface, which has a large diameter (i.e., 27.5 feet), the stringer feet are not in full contact with the IT surface. The flat-feet configuration for the IT installation can result in an inherent toes-up condition simply due to the stringer feet being flat and then installed on a cylindrical surface (i.e., in these FE models, toes are initially up approximately 18 mils, and the heels are up approximately 9 mils from the curved IT surface for the baseline flat-feet configuration). The stringer-feet imperfections and the fastener installation process are described next.

1. Stringer-Feet Imperfection Modeling

The fabrication of the IT external hat-shaped stringers is a multi-step process that starts with a sheet that is cold rolled to a general hat shape, and then hot formed to the specific dimensions and final shape. An added installation complication is that the stringer is fabricated with an upward bend on both ends to accommodate tapered IT chord flanges on the LOX and LH_2 ends of the IT. This bend occurs roughly at Fastener 7 for regions with a forward long chord*. From Fastener 7 to the front end, different stringer-feet imperfections may occur with the peak imperfection possibly occurring at the stringer ends and tapered linearly down to the flat-feet configuration at Fastener 7 (i.e., the imperfection is uniformly tapered over the flange chord length). The implication of this assumption is that stringer-feet imperfections have little or no influence on the response of Fastener 8 and beyond. A stringer foot has a heel (i.e., transition between foot and region close to the stringer sidewall) and a toe (i.e., region close to the stringer free edge) as shown in Fig. 7. The center of the fastener holes is 0.44 inches from the stringer free edge.

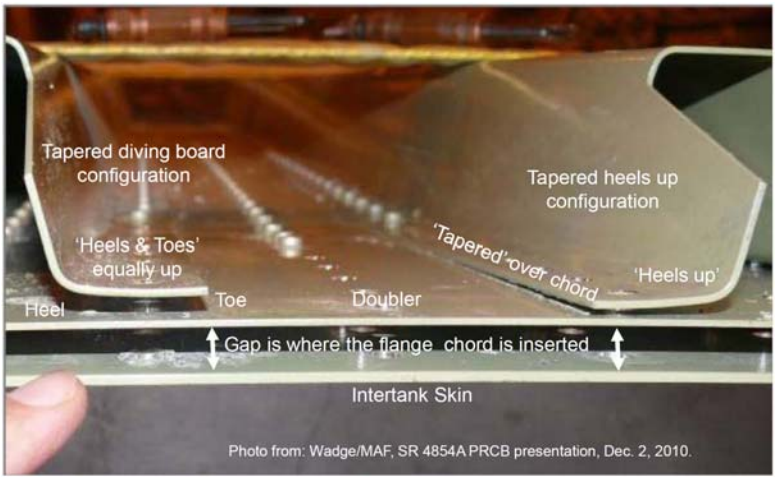

Figure 7. Various stringer-feet imperfections. Photograph courtesy of Mr. G. Wadge/LM-ET.

The baseline flat-feet configuration and three stringer-feet imperfection configurations are shown in Fig. 8. The baseline flat-feet configuration shown in Fig. 8a exhibits a toes-up condition due to the IT curvature. The heels-up configuration shown in Fig. 8b is defined as when the heels of the stringer feet at the end of the stringer are offset 60 mils further from the flat-feet configuration, while the stringer toes remain in the flat-feet configuration (linearly tapered across the stringer foot). In this configuration, the stringer toes are in the flat-feet configuration. The diving-board configuration shown in Fig. 8c has the heels and toes offset 70 mils from the flat-feet configuration (i.e., uniform offset with no tapering across the stringer foot). The toes-up configuration shown in Fig. 8d is when the toes of the stringer feet at the end of the stringer are offset 60 mils further away from the flat-feet configuration, while the stringer heels remain in the flat-feet configuration (linearly tapered across the stringer foot).

* The forward chord provides a flange for mating with the LOX tank. The length of the forward chord depends on the circumferential IT location: in some cases, it is a 'long' chord approximately 7 inches long, while in other location it is a 'short' chord approximately 5 inches long.

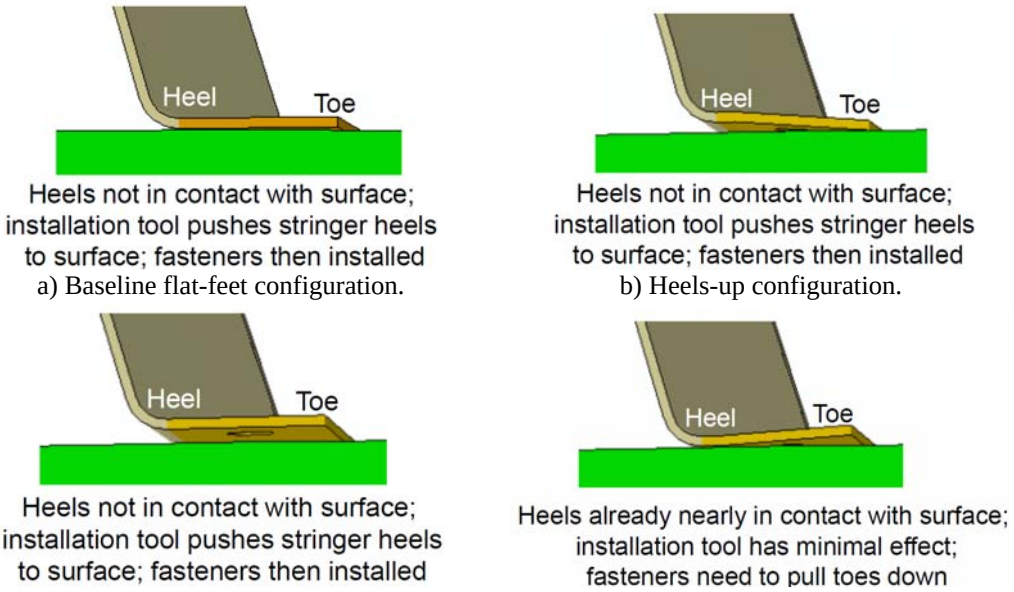

a) Baseline flat-feet configuration. b) Heels-up configuration.

c) Diving-board configuration. d) Toes-up configuration.

Figure 8. Baseline and three stringer-feet imperfection configurations.

The stringer configurations analyzed assume the same imperfection for both stringer feet. Imposing different stringer-feet imperfection types and/or imperfection amplitudes for the left and right stringer feet poses no additional analytical difficulty. However, a systematic approach to assess such a non-deterministic problem was not developed due to the lack of stringer-feet imperfection data.

2. Fastener Installation Simulation

The IT assembly process is understood to be as follows. First, align the stringer end at the LH_2 flange end. Then, rivets are installed from the center portion of the IT panel towards the ends. Next, the stringer hat near the stringer end is pushed down to the panel surface with a clamp screw assembly fixture shown in Fig. 9, and a drill jig is used to drill holes. The push-down displacement is dependent on the local stringer-feet configuration. Then, it is assumed that the Hi-lok® fasteners are installed after the rivets, followed by the installation of the four pairs of GP® lock bolts. During the preloading of the last pair of GP® lock bolts (i.e., Fastener 1), the stringer hat push-down displacement is removed from the analysis.

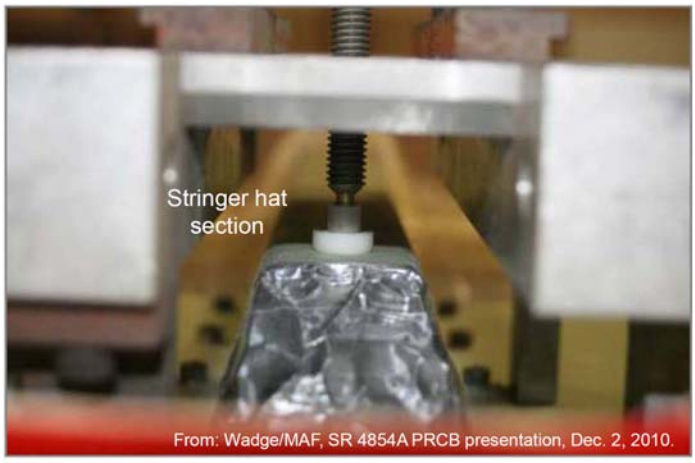

Figure 9. Stringer installation tool to push the stringer feet to IT surface.

The fastener installation simulation presented here attempts to mimic the assembly process just described. The single-stringer FE model is positioned over the IT panel FE model. After positioning the stringer, all rivets are installed (28 pairs of rivets for this FE model) and preloaded to 200 pounds in the simulation. This rivet preload value alleviated some of the numerical convergence issues that arose during the nonlinear iterations for the initial contact determination of these two independent FE models. Values of preload greater than 200 pounds for the rivets produced the same results. After the rivet installation is simulated, the push-down process is simulated by imposing a transverse applied displacement to a small central region on the stringer hat section outer surface approximately 0.5 inches from the end as indicated in Fig. 10. This rectangular region is defined by 18 surface nodes of ten adjacent solid element faces as indicated in Fig. 10, and covers an area of approximately 0.15 in^2. The minimum magnitude of the applied push-down

displacement in these simulations is at least 5 mils even for the flat-feet configuration. However, the value is dependent on the stringer-feet imperfection configuration.

Once the stringer is pushed down, three pairs of Hi-lok® fasteners are installed and preloaded to 2350 pounds. Subsequently, four pairs of GP® lock bolts are installed and preloaded to 3300 pounds. The last pair of GP® lock bolts are installed simultaneously as the applied push-down displacement is released in the analysis. At the end of this solution step, only the fasteners and the rivets are holding the stringer FE model to the IT segment FE model.

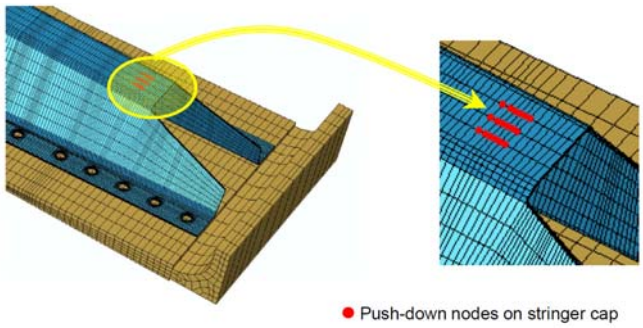

Figure 10. Location of the FE model push-down nodes.

B. Stringer Configurations Analyzed

Two stringer configurations are analyzed in this paper. One configuration has just the stringer attached to the IT panel, which is the baseline configuration as shown in Fig. 10, and is referred to, in this paper, as the configuration *without* the radius blocks. The second configuration is a configuration *with* the radius blocks installed at the ends of the stringer as shown in Fig. 11. The radius blocks are 0.19-inch-thick Al-2024 blocks 0.935 inches wide at the forward end and 0.85 inches wide at the aft end. They are used to stiffen the stringer feet against local bending. The radius blocks have two different lengths depending of the IT forward chord length: 4-hole or 6-hole radius blocks. In this paper, only the 6-hole radius blocks (6.19 inches long) and the IT forward long chord are analyzed. These 6-hole radius blocks are installed after the stringers have been fully installed on an IT panel by removing Fasteners 2 through 7 (four GP® bolts and two Hi-lok® fasteners), inserting the radius blocks, and installing new blind fasteners. Fastener 1 holds the stringer against the IT surface and is not removed during the radius block installation process.

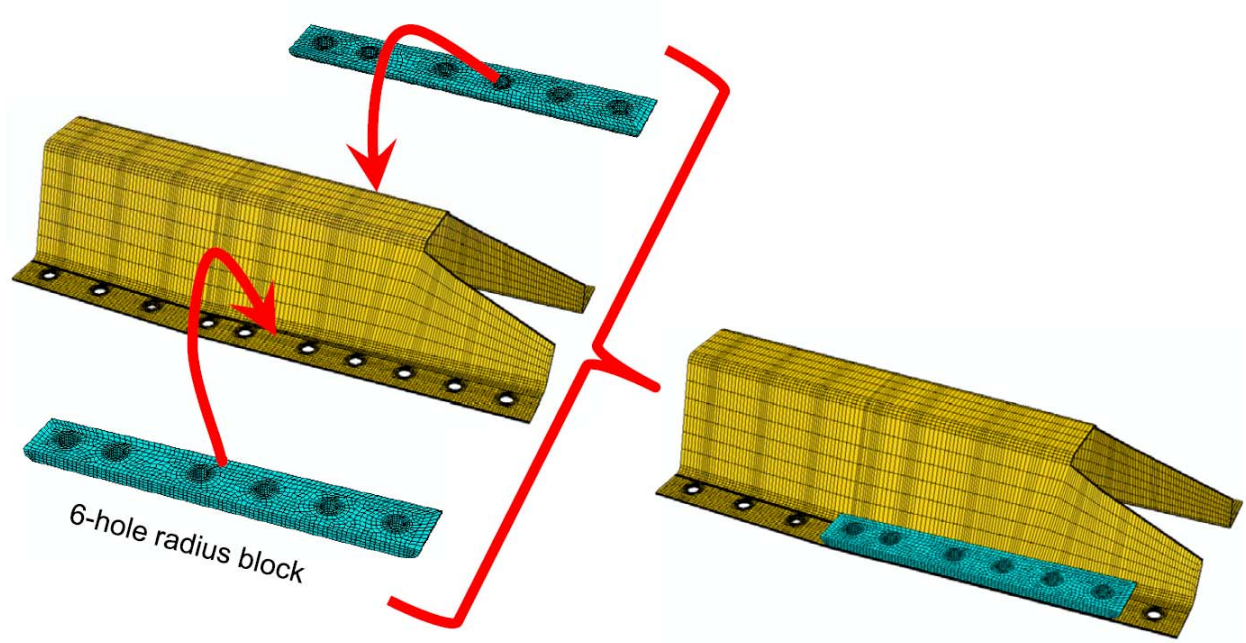

Figure 11. Installation of the 6-hole radius blocks over Fasteners 2 through 7.

C. Global Modeling Including Partial LOX Tank

The FE global model shown in Fig. 4 includes a portion of the LOX tank and the IT single-stringer model to simulate operating loads. The IT and stringer FE models are identical to the models used in the stringer-only simulations. The configuration and dimensions of the LOX tank aft of the forward T-ring frame were defined based on descriptions given in Refs. 3 and 4. The cylindrical barrel, aft Y-joint, weld lands, and aft elliptical dome were modeled using 12,841 C3D8 solid elements, while the aft spherical dome cap was modeled using 56 S4 shell

elements. The combined stringer-LOX tank model (referred to as the global model) has a total of 127,375 nodes and 86,355 solid elements. The LOX-tank FE model provides stiffness and load introduction to the IT stringer FE model for the thermal and mechanical operational loads and was not intended to be a stress analysis model for the LOX tank segments.

D. LOX Tank/IT Loading

External loads are imposed on the structure related to existing vehicle dead loads, increasing LOX mass during the fill or 'tanking' process, ullage pressure in the LOX tank, and ascent flight loads. Temperatures for the structural components of the global model are defined from the transient thermal analysis as the LOX tank is filled.[6] Typical loads acting on the LOX tank and IT are illustrated in Fig. 12.

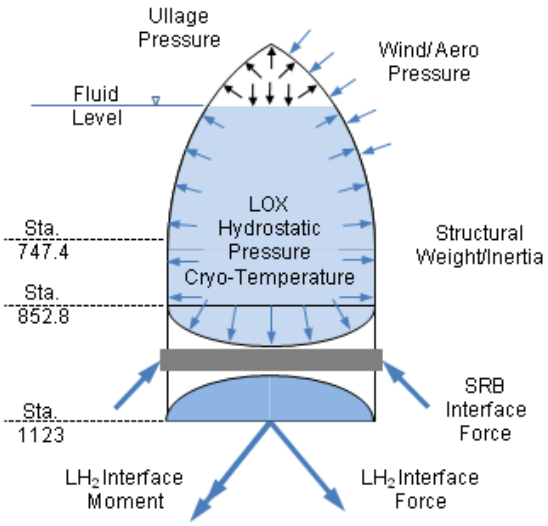

Figure 12. Typical LOX Tank and IT loading.

In addition to the hydrostatic pressure and thermal loads due to the cryogenic fluid in the LOX tank, other loads may be imposed related to the IT-to-LH_2 tank interface loads, LOX tank ullage pressure, external aerodynamic and/or wind pressures, and loads imposed by the SRBs through the IT cross-beam shown in Fig. 3. These loading events, which are described further in Appendix D of Ref. 2, are analyzed using a quasi-static approach wherein a series of 'snapshot' transient loading conditions are imposed on the structural model. In the quasi-static approach, the analysis results for each loading event provide the initial conditions for the subsequent loading event in a *quasi-static* time stepping manner. These events included:

- Assembly or fastener installation – This loading event was performed at room temperature and applies the fastener preloads in adjacent pairs of fasteners starting with the rivets from the aft end of the single-stringer model and proceeding forward until all rivets, Hi-lok® fasteners, and GP® lock bolts are installed. For cases involving the radius blocks, all fasteners are installed first, then Fasteners 2 through 7 are 'removed', the radius blocks are positioned, and the new radius block fasteners are installed.
- Pre-tanking – For this loading event, the ET is empty and ready for tanking operations to begin. An internal pressure is maintained to provide a positive tank pressure relative to the atmosphere. A running load is applied at the Y-joint, which encompasses the external wind loads and structural weight above station XT = 852.8. (Note that the Y-joint is shown in Fig. 4.)
- Tanking – This loading event is primarily a transient thermal loading event. The thermal response of the cryogenic fluid fill level of the LOX tank is simulated in a separate transient thermal analysis.[6] Fluid levels and corresponding temperature distributions are captured and applied to the structural model at 32 different times to provide time-consistent, quasi-static thermal environments and hydrostatic pressures during the LOX tank fill process. Eight of these snapshots of the temperature distribution during the tanking simulation are shown in Fig. 13. In this figure, an extended portion of the LOX tank FE model is included, and the displacements are scaled by a factor of five. An internal pressure attributed to the LOX ullage pressure is applied, as well as a running load applied to the Y-joint that encompasses the external wind loads and structural weight above station XT = 852.8. The ullage pressure and running load are bounding loads.

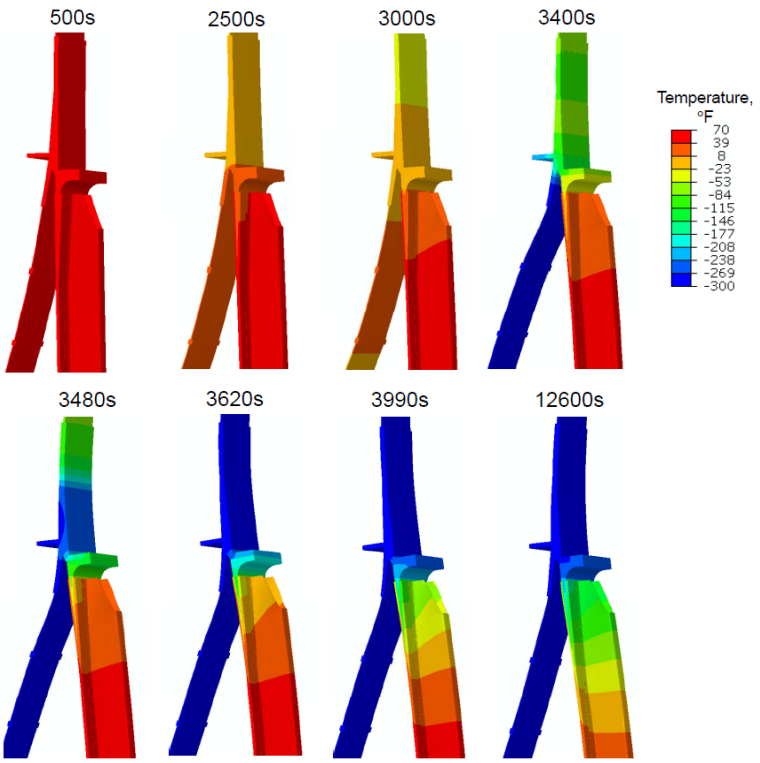

Figure 13. Eight snapshots of the temperature distribution during the tanking simulation imposed on the deformed shape of the global model – displacements scaled by 5. The time after starting LOX tanking of each 'snapshot' is indicated above each plot.

- Pre-launch – For this loading event, the LOX tank is full, and the Space Transportation System is ready for Space Shuttle Main Engine (SSME) ignition. The LOX tank and surrounding structure have reached thermal steady-state condition (i.e., temperature profile for 12600 seconds shown in Fig. 13). The tank pressure is modulated to provide a SSME-ignition pressure. The running load encompasses the external wind loads and the structural weight above station XT = 852.8.
- Flight – This load event starts with SSME ignition and continues through ET separation. The loading event considers the steady-state temperatures and head pressure for a full LOX tank, maximum and minimum ascent ullage pressure, and the running load is a bounding load that encompasses all other external loads and times through ET separation.

E. Boundary Conditions on Global Model

Symmetric boundary conditions were applied to the edges of the global 3D model shown in Fig. 4. The coordinate system of the edge surface nodes of the LOX tank barrel segment, elliptical aft dome segment, Y-joint segment, and IT chord/doubler/panel skin segment was transformed to a cylindrical coordinate system aligned with the ET axial direction. These nodes were restrained against translation in the tangential direction, which prevents rotation of the edge surfaces. The midplane of the aft spherical dome cap was modeled using shell elements and required translational and rotational restraints along the edges to impose a symmetric boundary condition. Nodes along the edges of the aft spherical dome cap were transformed to a spherical coordinate system with the origin located at the aft spherical dome cap center. These nodes were restrained against translation in the circumferential direction and rotation about the meridional direction, thereby imposing symmetric boundary conditions on the shell element portion of the global model.

Translational restraints along the ET axial (or XT) direction were applied to all nodes at the base of the IT panel skin segment and stringer. These translational restraints prevent the combined IT skin/stringer cross-section from rotating about the IT tangential axis. These boundary conditions define a symmetric slice or repeating element for the FE model. While the IT and LOX tank structures and loading are not periodic, and the configuration does not exhibit geometric symmetry, these assumptions provide a basis for parametric studies and are believed to provide bounding solutions.

F. Material Modeling

The IT material properties for aluminum lithium 2090-T83 were obtained from MSFC for room temperature and -25°F.[7] The elastic material properties are listed in Table 1, and the nominal uniaxial stress-strain curves for room temperature and -25°F are shown in Fig. 14. Data for the T-orientation are used in these analyses. Table 2 lists the Al 2195 material properties[8] used for the LOX tank components, and Table 3 lists the Al 2024-T81 material properties[9] used for the radius blocks. The analyses include the elastic-plastic, temperature-dependent stress-strain data for the IT components. The input to ABAQUS™ is the true stress as a function of plastic strain in a piecewise linear approximation for each specified temperature. Because the response is a single loading event with some, but not complete, load reversal expected, the response is a single cycle and isotropic strain hardening is assumed, and the influence of the Bauschinger effect is neglected. In addition, the material could be approximated as elastic, perfectly plastic in which case isotropic and kinematic strain hardening rules predict identical results.

Within a 3D stress analysis, the elastic-plastic response is assumed to be characterized by the uniaxial stress-strain data and requires effective stress and strain metrics to be defined and compared to a yield criterion. Once yielding is predicted, plastic flow occurs. In a multi-axis stress state, when the effective stress exceeds the initial uniaxial yield stress, yielding has occurred, and the subsequent local strain state will include elastic and plastic contributions. Once yielding is detected using the effective stress, the individual strain components will exhibit a plastic part even though the individual total mechanical strain components may be small enough to appear to be elastic because dislocations along other planes have occurred.

Table 1. Material properties for the IT stringers – nominal Al-Li 2090 T83.[7]

	Room Temperature	-25°F
Elastic modulus, Msi	11.5	11.8
Poisson's ratio	0.3	0.3
Coefficient of thermal expansion, in./in./°F	12.2×10^{-6}	11.7×10^{-6}

Table 2. Material properties for the LOX tank – Al 2195.[8]

	Room Temperature	-320°F
Elastic modulus, Msi	11.0	12.2
Poisson's ratio	0.3	0.3
Coefficient of thermal expansion, in./in./°F	12.6×10^{-6}	9.8×10^{-6}

Table 3. Material properties for the radius blocks – Al 2024-T81.[9]

	Room Temperature	-320°F
Elastic modulus, Msi	10.5	11.76
Poisson's ratio	0.33	0.33
Coefficient of thermal expansion, in./in./°F	12.2×10^{-6}	9.8×10^{-6}

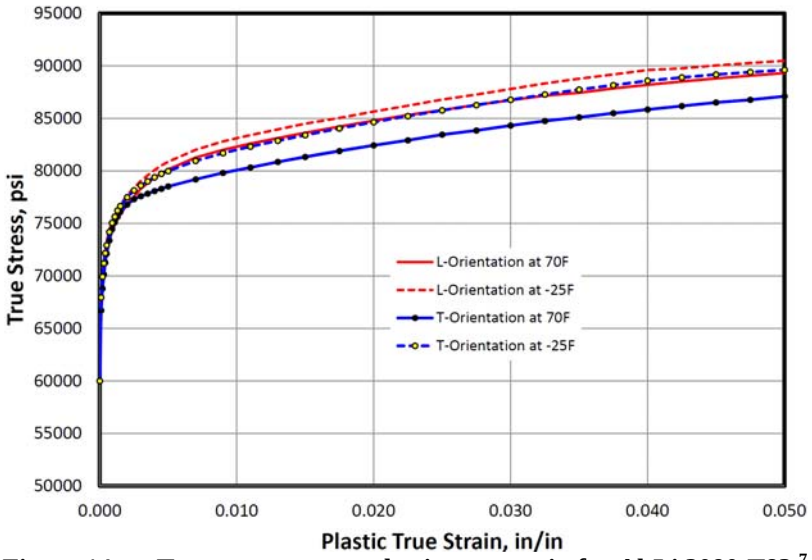

Figure 14. True stress versus plastic true strain for Al-Li 2090-T83.[7]

IV. Numerical Results and Discussion

The elastic-plastic, thermo-mechanical nonlinear structural response of the *global* model, based on a 2.5° slice of the IT skin and stringer with a partial LOX tank, to a series of operational thermal and mechanical quasi-static loads is presented. These simulations, performed using ABAQUS™, are all nonlinear analyses due to contact conditions between the IT segment and the stringer, the large-deflection response, and the elastic-plastic material behavior.

The following assumptions are made in these simulations:

- Linear taper of the stringer-feet imperfection while the stringer is over the forward long chord (over the first seven fasteners) with no imperfection beyond Fastener 8;
- Three types of stringer-feet imperfections (i.e., heels up, diving board, and toes up);
- An applied displacement on the stringer hat to push the stringer to the IT panel surface;
- Applied displacement magnitude defined by the distance the heels were initially displaced from the IT panel surface;
- Fastener installation in pairs from Fastener 8 location to Fastener 1 location;
- Maximum fastener preload values applied;
- Fastener head diameter of 0.389 inches; and
- Stringer thickness of 0.056 inches.
- IT panel skin thickness of 0.083 inches.
- Total double doubler thickness of 0.146 inches.

The flat-feet configurations are analyzed and discussed in this section. While the results for other stringer-feet configurations are presented in Refs. 2 and 10, a summary of the peak hoop strain results for each stringer-feet imperfection configuration is presented in the paper for three loading events.

A. Flat-feet Configurations

The baseline, flat-feet configuration shown in Fig. 8a is the nominal configuration for all stringers when installed on an IT panel. The thermo-mechanical stress analysis results from the global model are discussed in this section for the baseline, flat-feet configurations. Selected stress distributions predicted using the current 3D global FE analysis models are presented and compared. These results indicate that the hoop direction is the more critical direction, and therefore, hoop strain components are reported for the loading events. The hoop strain components include the total hoop strain, its elastic and plastic mechanical parts, and the thermal hoop strain.

First, the thermo-mechanical response for the baseline, flat-feet configuration *without* the 6-hole radius blocks installed is presented. Next, the response for the configuration *with* the radius blocks installed is presented and discussed. Then, the peak hoop strain results near the first fastener for the different loading events are compared for configurations *without* and *with* the radius blocks installed.

1. Configuration without Radius Blocks

The baseline, flat-feet configuration *without* the radius blocks installed is the basic configuration used for comparisons. In this configuration, the stringer feet are flat and would exhibit complete contact when placed on a flat surface. In the analysis model of the independent components (i.e., IT skin/chord/doublers and IT stringer), the flat-feet configuration of the stringer exhibits an inherent mild toes-up condition due to the curvature of the IT shell surface along the full length of the stringer model. The stringer heels are displaced from the IT surface by approximately 9 mils, and the toes are up approximately 18 mils. This initial geometric location of these surfaces in the FE models is to ensure the mathematical surfaces are independent and to mitigate any initial surface interpenetration caused by the FE meshing. Contact between the bottom of the stringer feet and the outer IT panel surface prevents penetration, and surface friction is included in the analyses.

After completing the assembly process, various operational loading events are imposed, and nonlinear thermo-mechanical solutions are computed for the global model. Following the assembly events, a total of 35 additional loading events are analyzed including the pre-tanking loading event, 32 snapshots from the thermal transient during the LOX tank tanking process, the pre-launch loading event, and the flight loading event.

IT flange rotation at the forward or LOX-tank interface, as depicted in Fig. 15, is another parameter monitored during the nonlinear analyses of the quasi-static loading events. A positive value of the flange rotation (a counter-clockwise or CCW rotation) would tend to ‘pull’ the IT skin away from the stringer feet. While the assembly process had only a marginal influence on IT flange rotation, the external loading events including the thermal transient due to filling the LOX tank are anticipated to generate positive flange rotation. Using a BOSOR finite difference axisymmetric shell analysis,[11] an IT flange rotation value of 0.0105 radians (0.602°) CCW at full flight

loading are reported in Ref. 12. Preliminary flange rotation results from the ET-137 tanking test in the range of 0.020-0.025 radians CCW are reported in Ref. 13.

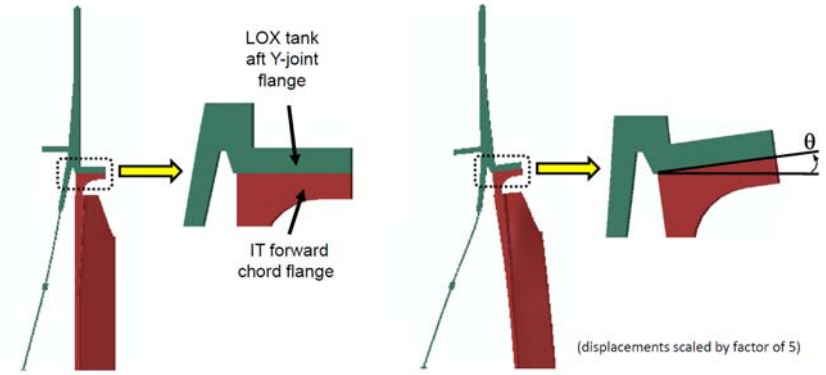

a) Undeformed configuration. b) Deformed configuration.

Figure 15. IT flange rotation schematic.

Qualitatively, the rotation of the IT chord flange has been previously found to occur due to the thermal gradient that develops during filling of the LOX tank (see Fig. 13). To quantify that influence, the flange rotation θ illustrated in Fig. 15 is calculated for each loading event from the global model simulation, and the results are shown in Fig. 16 for the baseline, flat-feet configuration *without* the radius blocks installed. The peak positive flange rotation* is approximately 1.58° (or 0.028 radians) CCW at 3620 seconds into the LOX tanking process, which agrees well with the value reported in Ref. 13.

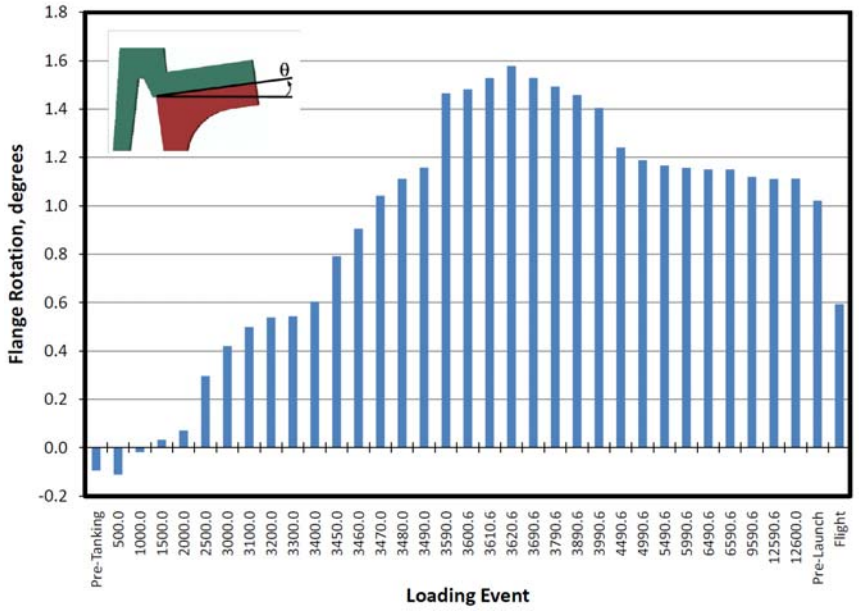

Figure 16. IT chord flange rotation for the flat-feet configuration *without* radius blocks installed for each loading event.

Stringer cross-sectional shapes with exaggerated displacements (scaled by a factor of five) are shown in Fig. 17 for several of the snapshot loading events analyzed. The orientation of the cross-sectional views is the same; however, as the thermal transient progresses, cryogenic shrinkage of the LOX tank occurs and thereby pulls the upper end of the stringer inward (i.e., 'downward' in the figure) making the stringer hat and feet more visible in the figure. Contours of the 'near' circumferential or hoop displacement component U2† are shown on the deformed shapes where the contour range is ±0.056 inches (i.e., deflections on the order of the stringer thickness). The U2 deflection values exceeding this range are shown as gray (greater than +0.056 inches) or black (more negative than –0.056 inches) in the contour plots.

* Positive values of θ mean that the IT flange is rotating CCW and moving away from the stringer.

† The U2 displacement component refers to the global coordinate system, which is nearly coincident with the circumferential or hoop direction given the large radius of the IT shell.

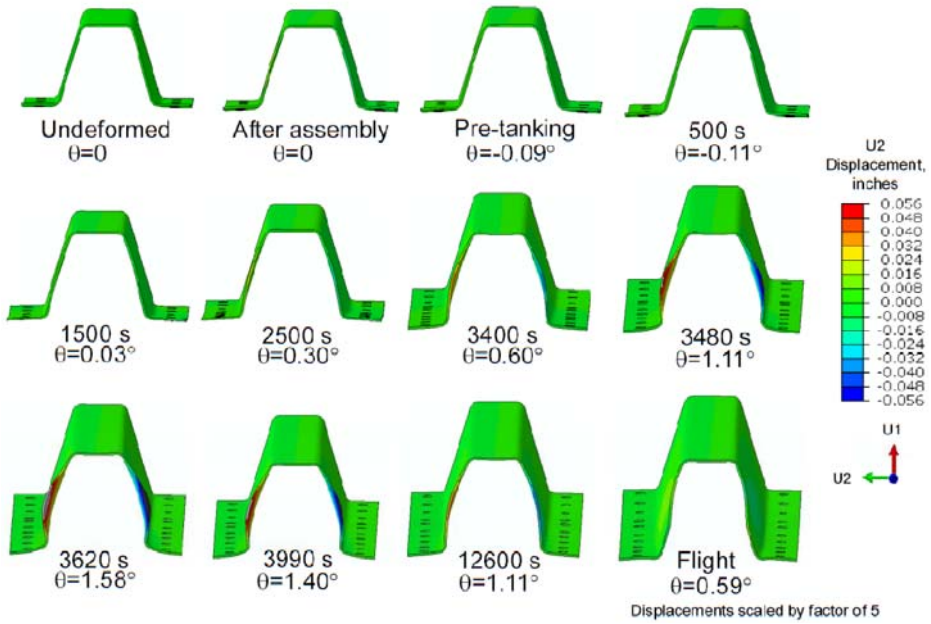

Figure 17. Deformed stringer cross-sectional shapes for the baseline, flat-feet configuration at different loading events.

After assembly, the IT flange rotation is zero, and only a slight outward transverse deflection of the stringer sidewalls is noticeable in the deformed shape and as indicated by the contour colors in Fig. 17. During the initial cool down portion of the transient thermal loading (i.e., first 500 seconds), the IT flange rotation is slightly clockwise rather than CCW. As the peak thermal gradient develops near 3620 seconds, the IT flange rotation reaches a peak CCW value, and the outward transverse sidewall deflections (U2) exceed the stringer thickness near the first three fasteners – the forward end of the stringer without a hat section. As the thermal transient continues to a steady-state condition, the IT flange rotation decreases, and the sidewall outward transverse deflections diminish. For the flight loading event, the sidewall deflections are barely noticeable.

As a result of the flange rotation response, the assembly step, the 3620-second snapshot in the tanking process, and the flight loading event were identified as key loading events to examine in more detail. Stress analysis results for these three loading events (after assembly, at 3620 seconds into tanking, and flight loading) are presented in Figs. 18 through 20, respectively, for the outer exposed surfaces of the stringer. In these figures, the normal stress components (i.e., radial, hoop, and axial directions) and the von Mises stresses are presented. The range of the stress contours is the same for all components and is fixed to be ±60,000 psi (i.e., the uniaxial initial yield stress).

The stress distributions after completion of the assembly step are shown in Fig. 18 for the flat-feet configuration *without* the radius blocks installed. The radial stress component shown in Fig. 18a represents the through-the-thickness stress component, with high compressive values near each fastener hole as expected due to the high fastener preload forces. The hoop and axial stress distributions shown in Figs. 18b and 18c, respectively, indicate very localized effects due to assembly alone. However, the von Mises stress distribution indicates a stress magnitude approaching the uniaxial initial yield stress value near the fastener holes (see Fig. 18d). Recall that in a combined stress state, only the effective or von Mises stress needs to exceed the uniaxial initial yield stress for the individual strain components to exhibit plastic strain.

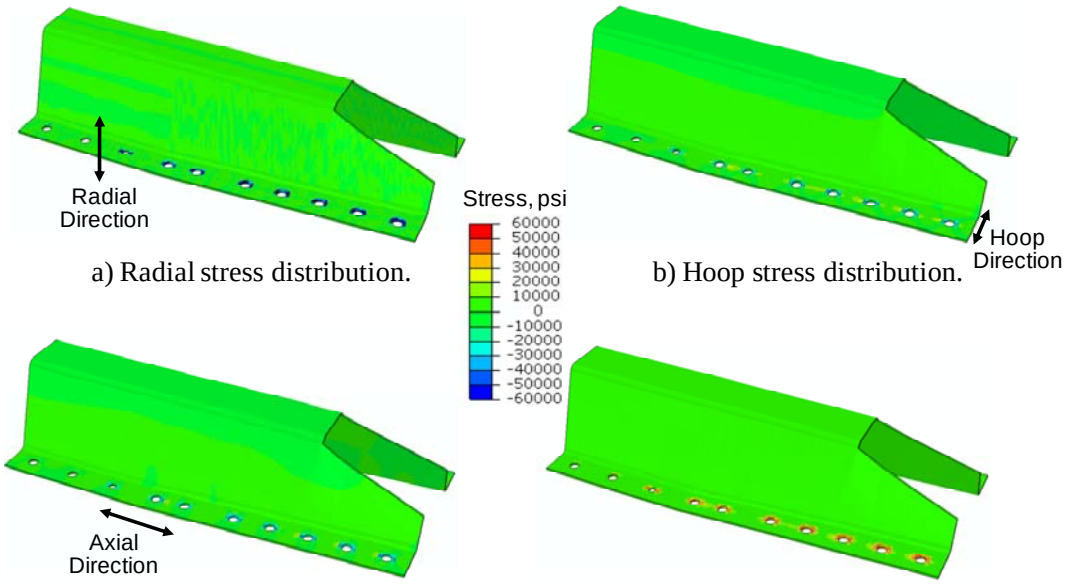

a) Radial stress distribution. b) Hoop stress distribution.

c) Axial stress distribution. d) Von Mises stress distribution.

Figure 18. Stringer stress contours by component after assembly for the flat-feet configuration *without* radius blocks installed.

The stress distributions at 3620 seconds after starting tanking are shown in Fig. 19 for the flat-feet configuration *without* the radius blocks installed. The radial stress component shown in Fig. 19a is essentially unchanged from the assembly step shown in Fig. 18a. As a result of the thermal gradient, the hoop stress component shown in Fig. 19b is significantly different from the assembly step. High compression values on the exposed surface of the stringer feet are noted along the first three fasteners, with a rapid transition from compression to tension as the stringer sidewall is approached. In addition, increased hoop stress levels are indicated near Fasteners 6 and 7 where the IT tapered chord ends. Tensile axial stresses are observed in Fig. 19c along the stringer hat (or cap), while high compressive values are noted near the first three fasteners. For the von Mises stress (a stress invariant), values exceeding the uniaxial initial yield stress are indicated in Fig. 19d by the gray regions in the contour plot near the first three fasteners.

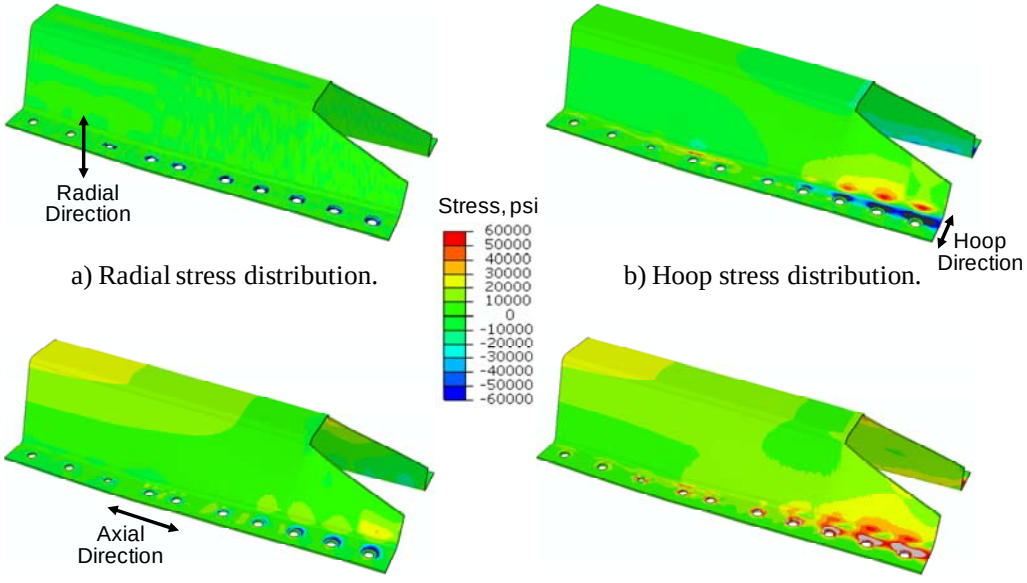

a) Radial stress distribution. b) Hoop stress distribution.

c) Axial stress distribution. d) Von Mises stress distribution.

Figure 19. Stringer stress contours by component at 3620 seconds after starting tanking for the flat-feet configuration *without* radius blocks installed.

The stress distributions for the flight loading event are shown in Fig. 20 for the flat-feet configuration *without* the radius blocks installed. In this case, the peak flange rotation decreased due to steady-state thermal condition and due to the flight running loads imposed on the aft Y-joint flange. Again, the radial stress distribution in Fig. 20a shows minimal change when compared with the previous two loading events. However, the hoop stress distribution in Fig. 20b has been relieved somewhat with peak compressive values occurring near Fasteners 3 through 5. The axial stress distribution shown in Fig. 20c increases in the stringer feet rather than just peaking at the fastener holes as indicated previously. Finally, the von Mises stress distribution shown in Fig. 20d indicates that elastic-plastic response in the stringer feet has developed further as evident by the increased size of the gray regions in the contour plot.

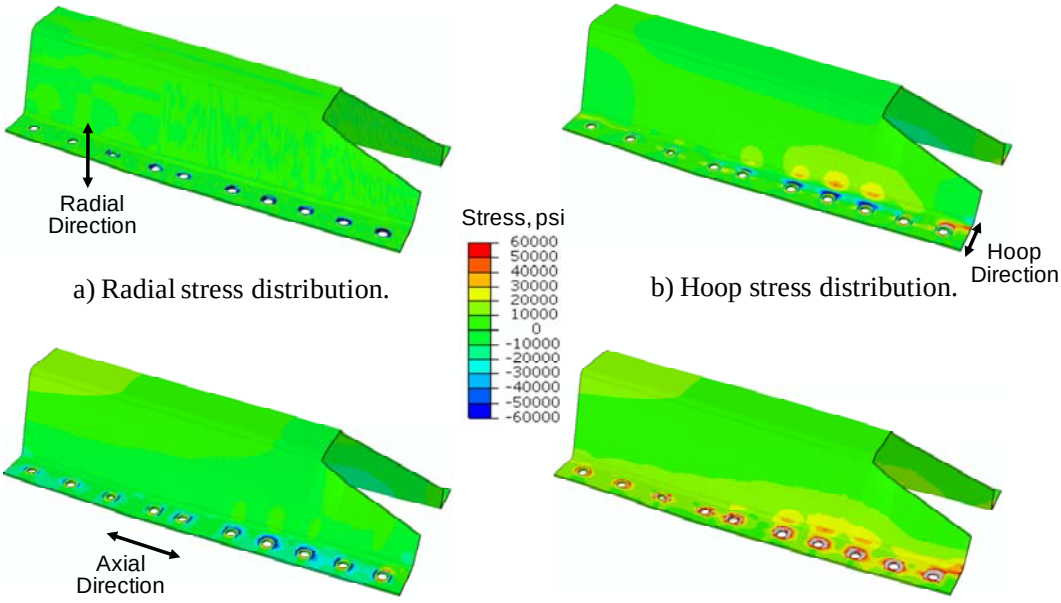

a) Radial stress distribution. b) Hoop stress distribution.

c) Axial stress distribution. d) Von Mises stress distribution.

Figure 20. Stringer stress contours by component with flight loading applied for the flat-feet configuration *without* radius blocks installed.

Since the original stringer failure mode was a through-crack presumably initiating on the bottom surface of the stringer feet and extending from Fastener 1 to Fastener 5 (e.g., see Refs. 1 and 2), a tensile hoop strain on the bottom surface of the stringer feet would tend to open any defect perpendicular to the hoop direction. Hence, to mitigate any risk associated with the possible use of suspect stringer material[*], it has been suggested that the strain levels in the stringer feet should not exceed the elastic limit.

The strain components extracted from the computational database at each of the eight element integration points within a solid element are compared, and the peak total strain value is identified within each fastener group of elements (i.e., each group of red elements highlighted in Fig. 21). The strains reported for the fastener assembly simulation are the total

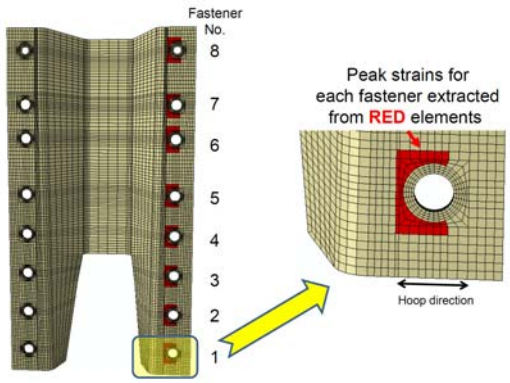

Figure 21. Selected element subgroups for strain recovery during the assembly simulation – red elements denote the fastener element group used to extract peak strain values near each fastener.

[*] Suspect stringer material refers to stringers fabricated from suspect material lots that while they met mechanical property requirements, exhibited anomalous microstructure in terms of excessive grain boundary precipitation, compared to control lots, suggesting off-nominal thermo-mechanical processing (high temperature and/or excessive time at temperature) resulting in poor fracture toughness without substantial influence on tensile properties. See Ref. 14 for more information.

strains, which is the sum of the elastic and inelastic components. For these analyses, the strain due to creep is neglected, and the inelastic strain represents only the plastic strain. The total hoop strain component is across the stringer feet in the circumferential or hoop direction of the IT shell (see Fig. 21). Positive hoop strain values on the bottom of the stringer feet would tend to 'open' a defect if and when it formed, and if the defect was aligned normal to the hoop direction. By selecting elements adjacent to but not under the fastener head (see the red elements indicated on the right side of Fig. 21), elements having peak through-the-thickness (or transverse normal) strains caused by preloading the fasteners are excluded from the direct comparison. However, all elements are automatically included in the contour plots to be shown. Large through-the-thickness normal stresses resulting from the fastener installation and preload conditions contribute to the effective or von Mises stress that is used to determine analytically the onset of local yielding.

Before presenting the results, the process used to extract these peak values needs to be described. Within each fastener group of elements as shown in Fig. 21, the results for each loading event are searched to identify the element integration point and element number having the peak plastic hoop strain for a specific fastener group. Once determined, the elastic, thermal, and the total strain components are extracted for that same element number and integration point. If the peak plastic hoop strain is zero, then the search is repeated looking for the peak total hoop strain. In subsequent bar-chart figures, the red bars denote the elastic part of the mechanical hoop strain, the blue bars represent the plastic part of the mechanical hoop strain, and the green bars represent the thermal hoop strain. In these figures, the red, blue, and green bars are stacked so that the individual height of a red or blue or green bar represents the hoop strain value for that part of the total strain. The tan bars in these figures represent the total hoop strain, which is the sum of the elastic, plastic, and thermal hoop strain components.

The peak hoop strain values shown in Fig. 22 are for the group of elements near the first fastener for each loading event analyzed using the flat-feet configuration *without* the 6-hole radius blocks. These hoop strain results indicate plastic strains occur near Fastener 1 after the initial installation of the stringer with flat feet. As the LOX tank filling process proceeds, the thermal gradient near the IT chord flange introduces significant cryogenic shrinkage that induced large plastic strains even though the thermal strain itself is small and compressive. The peak hoop strains occur after 3620 seconds into the tanking process. After 12600 seconds, steady-state thermal conditions exist for the IT. Mechanical loads due to prelaunch and flight are added to the steady-state thermal condition, and the resulting hoop strains are somewhat reduced due to the mechanical loads.

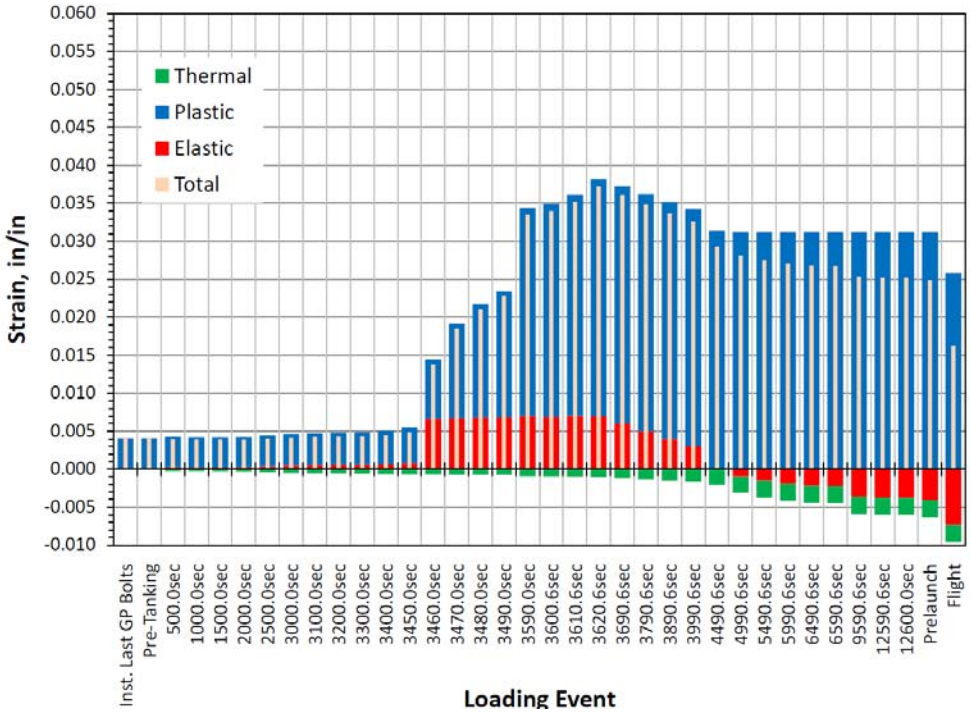

Figure 22. Peak hoop strains near Fastener 1 for the flat-feet configuration and different loading events: Without radius blocks installed.

2. Configuration with Radius Blocks

The flat-feet configuration *with* the 6-hole radius blocks installed is shown in Fig. 11 and represents the configuration along the LOX end of the IT panel with double doublers[*]. These 6-hole radius blocks are installed after the stringers have been fully installed on an IT panel by removing Fasteners 2 through 7, inserting the radius blocks, and installing new blind fasteners. Fastener 1 holds the stringer against the IT surface and is not removed during the radius block installation process. Plastic strains induced during the initial assembly of the stringer to the IT panel remain (are locked in) during the radius block installation. In the subsequent figures, the results shown after assembly are the assembly strains after the radius blocks have been installed.

The IT flange rotation θ illustrated in Fig. 15 is also calculated for each loading event using the flat-feet configuration *with* radius blocks, and the results are essentially the same as those shown in Fig. 16 for the baseline flat-feet configuration *without* radius blocks. The peak positive flange rotation is 1.58° (or 0.028 radians) at 3620 seconds into the LOX tanking process. These results indicate minimal influence of the radius blocks on the IT flange rotation for the flat-feet configuration.

Stress analysis results for the same three loading events (after assembly, after 3620 seconds into tanking, and flight loading) are presented in Figs. 23 through 25 for the outer exposed surfaces of the stringer. For clarity and ease of comparison to the results *without* the radius blocks shown in Figs. 18 through 20, the radius blocks are not shown in the subsequent stress contour plots. In these figures, the normal stress components (i.e., radial, hoop, and axial directions) and the von Mises stress are presented. The range of the stress contours is fixed to be ±60,000 psi (i.e., the uniaxial initial yield stress).

The stress distributions after completion of the assembly step (i.e., after the installation of the radius blocks) are shown in Fig. 23 for the flat-feet configuration *with* the radius blocks. The radial stress distribution shown in Fig. 23a represents the through-the-thickness stress component, with high compressive values near the first and eighth fastener holes due to the reduced fastener preload forces in Fasteners 2 through 7 when the radius blocks are installed. The hoop and axial stress distributions shown in Figs. 23b and 23c, respectively, indicate localized effects due to assembly. However, the von Mises stress distribution indicates a stress magnitude approaching the uniaxial initial yield stress value near Fasteners 1 and 8 (see Fig. 23d).

The stress distributions at 3620 seconds after starting tanking are shown in Fig. 24 for the flat-feet configuration *with* the radius blocks. The radial stress distribution shown in Fig. 24a is essentially unchanged from the assembly step. As a result of the peak thermal gradient, the hoop stress component shown in Fig. 24b is significantly different from the assembly step. However, the hoop stress levels are reduced compared to those predicted when the radius blocks are not installed (i.e., compare Figs. 24b and 19b). Tensile axial stresses are observed in Fig. 24c along the stringer hat, while compressive values are noted near the first three fasteners. For the von Mises stress, values exceeding the uniaxial initial yield stress are indicated by the gray regions in the contour plot near the first three fasteners. However, the presence of the radius blocks has reduced the overall stress level in the stringer feet (i.e., compare Figs. 24d and 19d).

The stress distributions for the flight loading event are shown in Fig. 25. In this case, the peak flange rotation decreased due to the steady-state thermal condition and due to the increased flight axial running load imposed on the aft Y-joint flange. The radial stress distribution in Fig. 25a shows minimal change when compared with the previous two loading events. However, the hoop stress distribution in Fig. 25b has been relieved with the peak compressive values occurring near Fasteners 3 through 5, which are under the radius blocks. The axial stress distribution shown in Fig. 25c extends further in the stringer feet and not just peaking at the fastener holes. Finally, the von Mises stress distribution shown in Fig. 25d indicates that elastic-plastic response in the stringer feet has developed, but appears to be more localized to regions around the fasteners. The region near Fastener 1 has the highest stress.

[*] Double doublers means that two doublers are present at this location. A larger one that is 0.090 inches thick and a smaller one that is 0.056 inches thick.

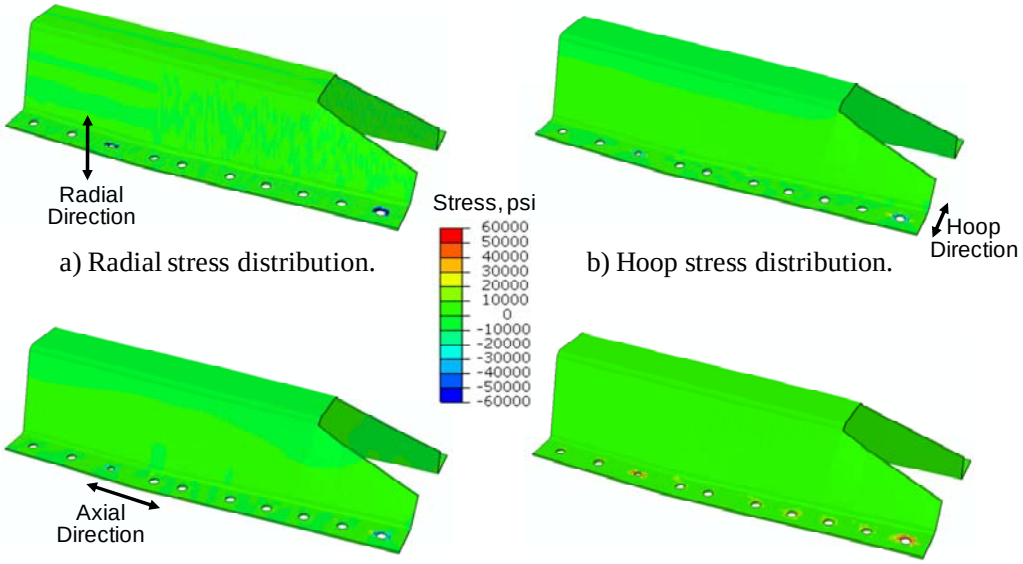

a) Radial stress distribution. b) Hoop stress distribution.

c) Axial stress distribution. d) Von Mises stress distribution.

Figure 23. Stringer stress contours by component <u>after radius blocks are installed</u> for the flat-feet configuration *with* radius blocks. Stress values plotted as gray exceed the maximum tensile value, and values plotted as black exceed the maximum compressive value.

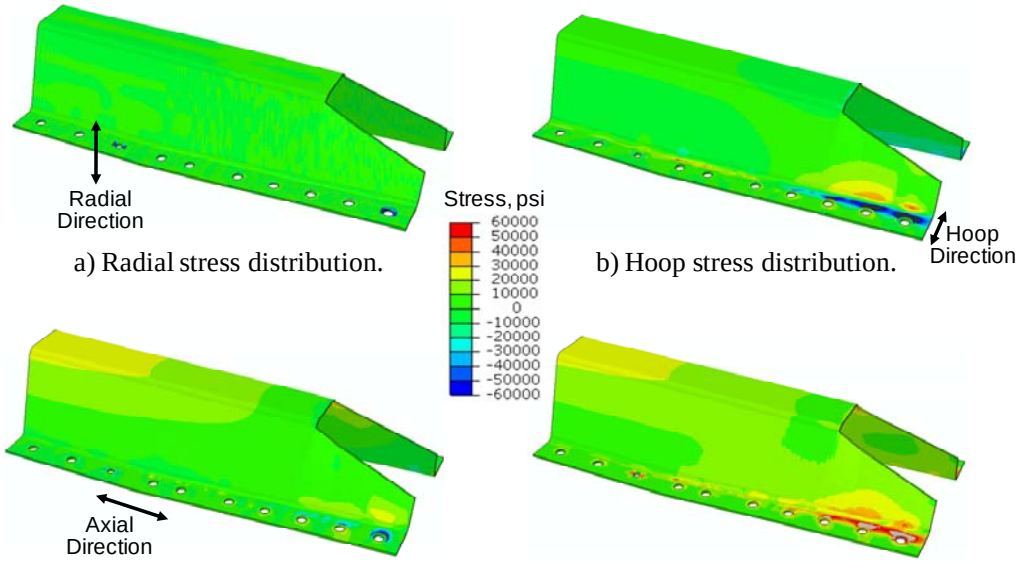

a) Radial stress distribution. b) Hoop stress distribution.

c) Axial stress distribution. d) Von Mises stress distribution.

Figure 24. Stringer stress contours by component <u>at 3620 seconds after starting tanking</u> for the flat-feet configuration *with* radius blocks. Stress values plotted as gray exceed the maximum tensile value, and values plotted as black exceed the maximum compressive value.

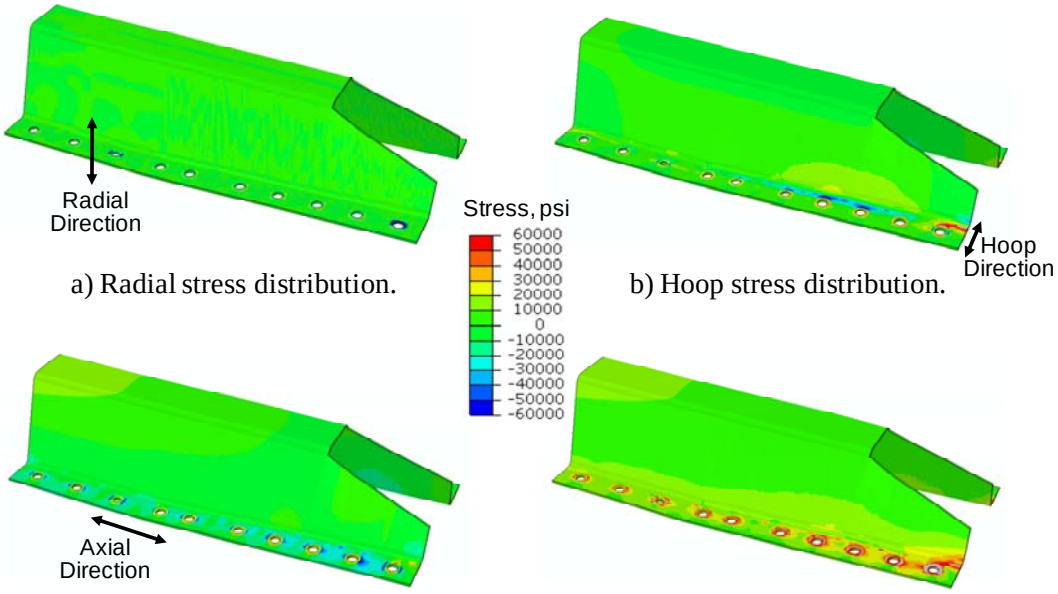

a) Radial stress distribution. b) Hoop stress distribution.

c) Axial stress distribution. d) Von Mises stress distribution.

Figure 25. Stringer stress contours by component <u>with flight loading applied</u> for the flat-feet configuration *with* radius blocks. Stress values plotted as gray exceed the maximum tensile value, and values plotted as black exceed the maximum compressive value.

The peak hoop strain values shown in Fig. 26 are for the group of elements near the first fastener and for each loading event analyzed using the flat-feet configuration *with* the 6-hole radius blocks. These hoop strain results indicate plastic strains occur near Fastener 1 after the initial installation of the stringer with flat feet and not due to the installation of the radius blocks. The peak hoop strains again occur after 3620 seconds into the tanking process. After 12600 seconds, steady-state thermal conditions exist for the IT. Comparison of these results *with* the radius blocks installed to those in Fig. 22, *without* the radius blocks installed, reveals that the radius blocks do reduce the peak strain levels for the operational loading events.

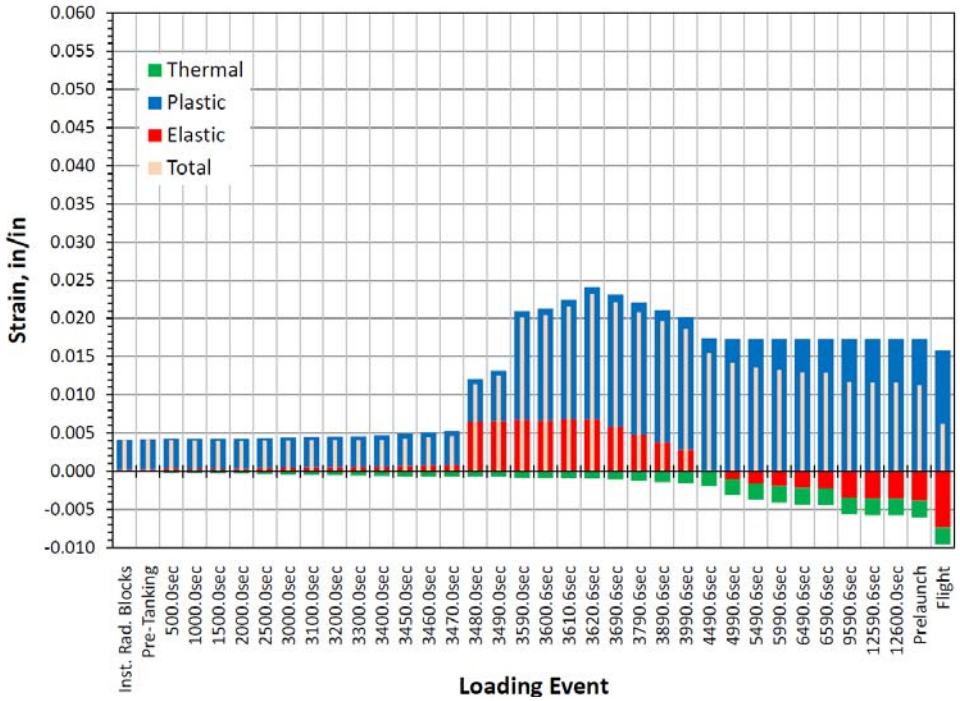

Figure 26. Peak hoop strains near Fastener 1 for the flat-feet configuration and different loading events: With radius blocks installed.

3. Peak Hoop Strain Comparisons without and with Radius Blocks

A tensile hoop strain on the bottom surface of the stringer feet would tend to open any defect perpendicular to the hoop direction. In particular, it has been suggested that the strain levels need to remain elastic to mitigate any risk associated with the possible use of suspect material in the stringers. Previously in Figs. 22 and 26, the peak hoop strain values for the flat-feet configuration *without* and *with* the 6-hole radius blocks installed are presented near Fastener 1 for each loading event analyzed. The maximum peak hoop strain values occur during the tanking process after 3620 seconds and not during the assembly step. The thermal hoop strains are small and compressive due to the change in temperature for the stringer feet; however, the mechanical loading in the stringer feet due to IT flange rotation caused by cryogenic shrinkage of the IT is a primary contributor to the hoop strain. The peak hoop strains from the flight loading conditions are bounded by the peak strains from the tanking simulation. The presence of the radius blocks tends to reduce the peak hoop strains near Fastener 1.

The peak hoop strains near the first eight fasteners are shown in Figs. 27 and 28 for the four key loading events. The peak hoop strains for the stringer feet *without* the radius blocks are shown in Fig. 27. Peak values from each loading event are shown for each fastener region. With the exception of Fastener 8, each fastener region exhibits plastic strain with the higher values being near the first four fasteners, and the highest hoops strains occur near Fastener 1. The peak hoop strains for the stringer feet *with* the radius blocks are shown in Fig. 28. Again, peak values from each loading event are shown for each fastener region. Similar trends are seen in these results compared to the results *without* the radius blocks. However, the peak values are significantly reduced. Note that any plastic strain induced during the initial assembly remains locked in as the radius blocks are installed.

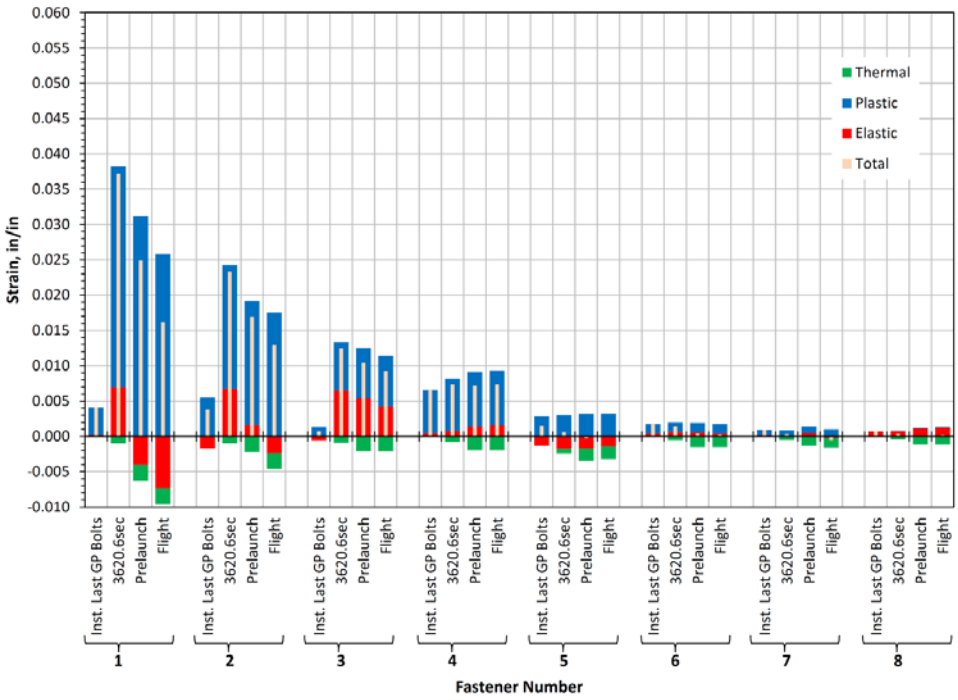

Figure 27. Peak hoop strains near the first eight fasteners for the four key loading events using the flat-feet configuration – without radius blocks installed.

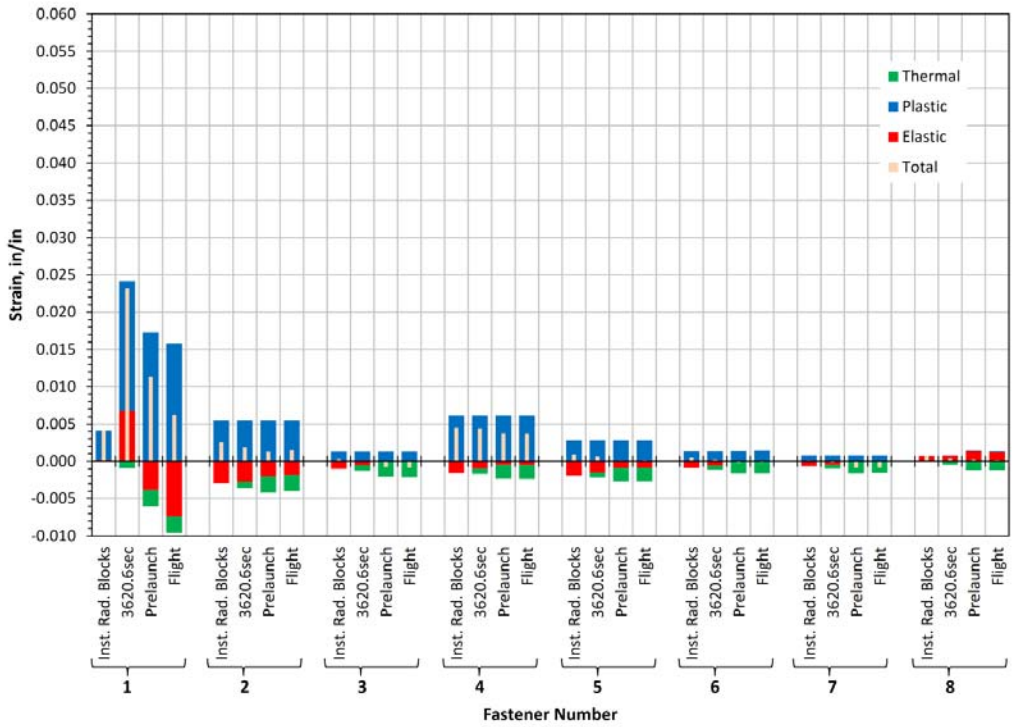

Figure 28. Peak hoop strains near the first eight fasteners for the four key loading events using the flat-feet configuration – with radius blocks installed.

A final observation is related to the different response expected near Fasteners 1, 2, and 3 compared to the other fasteners. The first three fasteners on the stringer are over a region where the stringer has no cap and its sidewalls are tapered in height as shown in Fig. 11. Because of the additional flexibility in this region, higher peak strains develop for the thermal and mechanical loading events. When the radius blocks are installed, the region near Fastener 1 is unsupported by the radius blocks and continues to exhibit higher peak strains than the remaining fasteners. However, those peak values are smaller than the peak values predicted when the radius blocks are not installed.

B. Stringer-Feet Imperfection Configurations

The flat-feet configuration of the stringer feet has been primary focus of this paper. Stringer-feet imperfection studies have also been performed, and the results are summarized in Tables 4, 5, and 6. The peak total hoop strains near Fastener 1 are tabulated for the four stringer-feet configurations (i.e., flat-feet, heels-up, diving-board, and toes-up configurations) after assembly in Table 4, after 3620 second into tanking in Table 5, and under flight loading in Table 6. Values *without* and *with* the radius blocks installed are reported. Ratios of the total hoop strain *without* radius blocks to total hoop strain *with* radius blocks are also reported, where values greater than unity indicate the radius blocks reduce peak hoop strains.

Results in Table 4 indicate that the stringer imperfection configuration that generated the largest assembly strains is the toes-up condition, which is reported as an unlikely condition. However, all assembly simulations resulted in plastic hoop strains developing in the first seven fasteners. Plastic strains induced during assembly are locked in for subsequent loading events.

Results in Table 5 indicate that all stringer-feet configurations result in high total hoop strains after 3620 seconds into tanking. At this time, the cryogenic LOX fluid level has reached the IT forward chord flange level, causing the large flange rotation. All three stringer imperfection configurations exhibit higher total hoop strains than the flat-feet configuration; however, the hoop strain values for the flat-feet configuration without the radius blocks approach four percent strain. Installation of the radius blocks does reduce the total hoop strain.

Results in Table 6 indicate that the mechanical loading induced by flight loads imposed at the IT forward chord flange reduce the peak hoop strain levels. These mechanical loads tend to restore the IT forward flange region to its original cylindrical shape from the inward bending caused by cryogenic shrinkage during tanking. Again, the radius blocks tend to reduce the total hoop strain.

Table 4. Summary of peak total hoop strain predictions near Fastener 1 after the assembly/installation process.

Stringer Feet Configuration	Total hoop strain for Fastener 1 element group, in./in.		Ratio of total hoop strain without radius blocks to strain with radius blocks
	Without radius blocks	With radius blocks	
Flat-feet	0.0041	0.0041	1.000
Heels-up, 60-mils	0.0025	0.0050	0.500
Diving-board, 70-mils	0.0025	0.0025	1.000
Toes-up, 60-mils	0.0234	0.0243	0.963

Table 5. Summary of peak total hoop strain predictions near Fastener 1 at 3620 seconds into the tanking process.

Stringer Feet Configuration	Total hoop strain for Fastener 1 element group, in./in.		Ratio of total hoop strain without radius blocks to strain with radius blocks
	Without radius blocks	With radius blocks	
Flat-feet	0.0372	0.0232	1.603
Heels-up, 60-mils	0.0579	0.0435	1.331
Diving-board, 70-mils	0.0569	0.0405	1.405
Toes-up, 60-mils	0.0535	0.0479	1.117

Table 6. Summary of peak total hoop strain predictions near Fastener 1 under flight loading conditions.

Stringer Feet Configuration	Total hoop strain for Fastener 1 element group, in./in.		Ratio of total hoop strain without radius blocks to strain with radius blocks
	Without radius blocks	With radius blocks	
Flat-feet	0.0162	0.0062	2.613
Heels-up, 60-mils	0.0331	0.0181	1.829
Diving-board, 70-mils	0.0309	0.0171	1.807
Toes-up, 60-mils	0.0396	0.0362	1.094

Concluding Remarks

Elastic-plastic, large-deflection nonlinear stress analyses were performed for the external hat-shaped stringers (or stiffeners) on the IT portion of the Space Shuttle's ET. These stringers are subject to assembly strains when the stringers are initially installed on an IT panel. Four different stringer-feet configurations including the baseline flat-feet, the heels-up 60-mil, the diving-board 70-mil, and the toes-up 60-mil configurations were examined analytically using the stringer-push-down assembly procedure and operational loading events. The von Mises stress distributions after assembly indicated that localized plasticity develops around the first seven fastener pairs.

To assess the effect of stringer assembly and plasticity on the response, four different stringer-feet configurations were examined analytically using the stringer push-down assembly procedure: baseline flat-feet, heels-up 60-mil, diving-board 70-mil, and toes-up 60-mil. Only the toes-up 60-mil configuration resulted in high assembly strains. However, all configurations exhibited plastic hoop strains in the stringer feet due to assembly. The magnitude of the assembly strain was determined not to be additive to the strain resulting from the operational loading events. Nonlinear response smears the effect of assembly; i.e., low assembly strain does not necessarily result in lower peak strain response.

Thermal loading due to tanking was verified to be the bounding operational loading event examined for the forward end of the IT stringer. The cryogenic shrinkage caused by the tanking event resulted in a rotation of the IT flange towards the IT center, which in turn loads the IT stringer feet. Peak hoop strain levels were predicted to be in the range expected for local stringer failures to occur. The analyses suggested that the strain levels at the first three fasteners remained sufficiently high so that a failure may occur during LOX tanking if a rogue stringer[*] were present. The peak hoop strains decreased beyond Fastener 3 due to the presence of the stringer cap. Absence of the cap increased the local sidewall flexibility resulting in large transverse sidewall deflections that generate a bending load in the stringer feet.

[*] A rogue stringer is defined as a stringer fabricated using suspect heat treatment lot of material and/or having potential stringer-feet imperfections when installed on a cylindrical surface.

The analyses confirmed that the radius block modification increased the apparent capability of the stringers on the LOX tank end of the IT. While the installation of radius blocks reduced the peak strains, the strain level remained sufficiently high so that a failure may occur if a rogue stringer were present. The radius blocks do indicate an increase in capability, but do not eliminate the possibility of a local stringer failure.

References

[1]Gentz, S. J., "Space Transportation System (STS)-133/External Tank (ET)-137 Intertank (IT) Foam Crack and Repair Assessment," NESC-RP-10-00680, 2012. (Also available as NASA/TM-2012-217338, February 2012.)

[2]Knight, N. F., Jr., Song, K., Elliott, K. B., Warren, J. E., and Raju, I. S., "Space Transportation System (STS)-133/External Tank (ET)-137 Intertank (IT) Foam Crack and Repair Assessment: Elastic-Plastic Thermo-Mechanical Nonlinear Structural Analyses," NASA TP, 2012.

[3]Anon., *Space Shuttle External Tank System Definition Handbook, Volume II Layout Drawings*, LMC-ET-SE61-1, DR SE61 WBS 3.6.6, NAS8-26200, December 1997.

[4]Nemeth, M. P., Britt, V. O., Collins, T. J., and Starnes, J. H., Jr., "Nonlinear Analysis of the Space Shuttle Superlightweight External Fuel Tank," NASA TP-3616, December 1996.

[5]Anon., *ABAQUS/Standard User's Manuals, Version 6.10*, Dassault Systèmes Simulia Corp., Providence, Rhode Island, 2010.

[6]Rickman, S. L., "Space Transportation System (STS)-133/External Tank (ET)-137 ET Foam Crack and Repair Assessment: Thermal Analysis Report," NASA/TM-2011-217306, November 2011.

[7]Burkholder, J. T., "Calculation of Average Stress-Strain Curve for Al-Li 2090-T83 ET Stringer Material," MSFC M&P Laboratory, Flash Report No. MPFR-11-004, March 23, 2011.

[8]Anon., "ET Project – Design Values for Aluminum Alloy 2195," Report MMC-ET-SE64-H, Drawing No. 809-3510, Lockheed Martin Michoud Space Systems, April 1999.

[9]Anon., *Military Handbook: Metallic Materials and Elements for Aerospace Vehicle Structures*, MIL-HDBK-5H, Section 3.2.3, December 1, 1998.

[10]Knight, N. F., Jr., Song, K., Elliott, K. B., Raju, I. S., and Warren, J. E., "Elastic-Plastic Nonlinear Response of a Space Shuttle External Tank Stringer: Part 1 – Stringer-Feet Imperfections and Assembly," AIAA Paper to be presented at the *53rd AIAA/ASME/ASCE/ATTS/ASC Structures, Structural Dynamics, and Materials (SDM) Conference*, Honolulu, Hawaii, April 23–26, 2012.

[11]Bushnell, D., "Stress, Stability, and Vibration of Complex Branched Shells of Revolution: Analysis and User's Manual for BOSOR4," NASA CR-2116, October 1972.

[12]Wadge, G., "2.2 – Design Analysis Skin/Stringer NASTRAN Finite Element Model Analysis Summary," presentation at the *MAF Technical Interchange Meeting*, January 13-14, 2011.

[13]Oliver, S., "LO_2 Flange Rotation and Displacement Using Photogrammatry Data from Tanking Test – Panel 6," MSFC presentation charts, January 26, 2011.

[14]Piascik, R. S., "Space Transportation System (STS)-133/External Tank (ET)-137 ET Foam Crack and Repair Assessment: Proximate Cause Determination and Material Characterization Study," NASA/TM-2011-217318, December 2011.